PNAS

www.pnas.org

Supplementary Information for

The impact of climate change on the transition of Neanderthals to modern humans in Europe

Michael Staubwasser, Virgil Drăgușin, Bogdan P. Onac, Sergey Assonov, Vasile Ersek, Dirk L. Hoffmann, Daniel Veres

Michael Staubwasser
Email: m.staubwasser@uni-koeln.de

This PDF file includes:

> Supplementary text
> Figs. S1 to S4
> Tables S1 to S2
> References for SI reference citations

Other supplementary materials for this manuscript include the following:

> Datasets S1

Supplementary Information Text
Materials and Methods.

Figure S1 shows the location of paleoclimate and environmental records used for comparison, in addition to archaeologic sites discussed in the text. The two speleothems presented in this study are from two sites in the East and South Carpathians. Tăușoare Cave (TC) is situated in the Rodnei Mountains of the East Carpathians, northern Romania (47º 26' N, 24º 31' E), at an altitude of 950 m. The cave has a surveyed length of over 8.5 km and is 329 m deep and hosts an abundance of gypsum crusts and flowers along with the presence of various mixed cation sulfates [1, 2]. Sulfate derives from weathering of pyrite present in the calcite and bituminous sediments. The process provides significant acidity for calcite dissolution in this cave. Thus, the isotopic composition of the host-rock calcite rather than soil CO_2 dominates the $\delta^{13}C$ record of TC speleothems. Stalagmite 1152 was retrieved from the "Dining Room" at about 625 m from and about 190 m below the entrance. It is 27 cm long and is made of dark-brown dense calcite (Fig. S2). The growth axis of stalagmite T-1152 is stable for the first 23 cm and changes direction for the last 4 cm. Ascunsă Cave (AC) is situated in the Mehedinți Mountains, South Carpathians, southwestern Romania, at an altitude of 1050 m (45º 00' N, 22º 36' E). The cave is 400 m long and over 200 m deep, formed mostly on the contact between Barremian-Aptian limestone and Turonian-Senonian wildflysch (melange) [3]. Stalagmite POM1 was retrieved from the "White Chamber", at about 80 m from the entrance. It is ~30 cm long and composed of alternations of dense dark calcite and lighter, less dense calcite (Fig. S2). The growth axis presents several slight direction changes.

For U-Th dating, samples were drilled parallel to growth layers. U and Th were analyzed by MC-ICP-MS (Neptune+, Thermo) after adding a $^{229}Th – ^{236}U$ double spike and subsequent ion-exchange chromatographic separation of U and Th from the sample matrix [4] (Tab. S1). A detrital Th-correction was applied assuming the average crustal $^{232}Th/^{238}U$ activity ratio of 1,250 ± 0.625. Detrital ^{230}Th correction amounts to within 50 – 350 years for the AC-speleothem, and 10 – 260 years for the TC-speleothem. The final chronology was modeled using the STALAGE software package [5]. Results can be found in Dataset S1.

For stable C and O isotope ratios samples were drilled continuously at 250 µm (TC) and at 300 µm (AC) resolution and analyzed by gas-IRMS (Thermo 253, and Thermo Delta+) at the University of Cologne and (TC) and the University of South Florida (AC). Results can be found in Dataset S1. The commonly applied 'Hendy-Test' to exclude kinetic domination of isotope fractionation was not performed. Both speleothems show relatively low growth rates and poor resolution of growth layering at the 250 - 300 µm sampling resolution level. The criterion of the Hendy-Test is to look for covariance of $\delta^{13}C$ and $\delta^{18}O$ within the same growth layer, which may hint at potential kinetically dominated isotope fractionation as a result e.g. of rapid degassing or rapid calcite precipitation. Because the two speleothems generally show little covariance between $\delta^{13}C$ and $\delta^{18}O$ overall, the criterion to meet the Hendy-Test is essentially fulfilled. In addition, cave monitoring water isotope data (δD, $\delta^{18}O$) suggests that oxygen isotopes fractionate at equilibrium between drip water and calcite, and carbon isotopes may at the worst contain a kinetic fractionation of 1.0 - 1.5 ‰ [6].

Regarding the association of the TC-stalagmite's pronounced low $\delta^{18}O$ interval between ~ 40.7 and 39.7 ka with GS-10 (between 40.8 and 40.2 ka in the GICC05 chronology) [5], as opposed to an association with GS-9 – H4 (between 39.9 and 38.2 ka in the GICC05 chronology), it is worthwhile to assess potential chronologic inaccuracy due to the correction for detrital Th. The onset of the low $\delta^{18}O$ has been dated directly to 40.66 ± 0.47 ka (40.92 ± 0.47 ka without detrital Th correction) (Tab. S1). An activity ratio for $^{230}Th/^{232}Th$ of 101 suggests a small detrital contribution – amounting to an age correction of ~ 260 years. However, detrital ^{230}Th just

amounts to ~0.5% of the total measured ^{230}Th activity based on the average crustal Th/U activity ratio (1.20) for a detrital contamination. To bring the resulting 40.7 ka onset age in line with the 39.9 ka BP onset age of GS-9 – H4 would require a low detrital Th/U ratio of less than 0.4, well outside the lower boundary for crustal Th/U of 0.625 and unusual for the given setting.

The Ascunsă Cave δ^{18}O record

Stable O-isotopes combine information on temperature and a number of hydrologic aspects that may be constrained by data comparison in regional and temporal context. Throughout the Holocene, the amplitude of δ^{18}O variability in the western Mediterranean, the Alps, and northern Romania – including TC – was significantly lower (~ 0.5 ‰) than in the eastern Mediterranean and southern Romania – including AC (7). An even larger amplitude difference between the AC-δ^{18}O and the TC-δ^{18}O existed during MIS-3. (Fig. S3). This cannot be explained by a different temperature regime alone (see main article) but must reflect a significant hydroclimatic contribution to the AC speleothem δ^{18}O records. The pacing of δ^{18}O is very different between AC and TC, and between AC and Greenland temperatures (8, 9). Thus, it is unlikely, that the two speleothems were inside the same hydrologic regime but record latitudinal differences in rain-out history from the same source. However, there is a similar structure between AC-δ^{18}O record and eastern Mediterranean marine and speleothem records (Fig. S4) (10). This pattern-similarity between the AC-δ^{18}O record and the eastern Mediterranean is observed only when the AC-stalagmite's δ^{18}O record is plotted with an inverted scale relative to the speleothem record from the Levant (Fig. S4). Numeric climate simulations of the last glacial (11) demonstrate the underlying causality for this apparent inverse correlation between the East Carpathians and the Eastern Mediterranean. All simulated modes of atmospheric circulation patterns that contributed to the average glacial precipitation over European and the Mediterranean show seasonal precipitation anomalies of opposite sign between the eastern Mediterranean and east-central Europe. This synoptic-scale relationship is corroborated by a similar relationship between the speleothems of AC and Karaca Cave (12), eastern Turkey.

Interstadial GI-7 stands out in the AC-δ^{18}O record with an anomalous isotope event (Fig. S3), a minimum more than 1 ‰ lower than all other features in the record. It is also a prominent feature in the speleothem and marine records from the eastern Mediterranean (Fig. S4). This could suggest that supply and influence of Mediterranean moisture in the region of the South Carpathians was highly variable between interstadials. Although the loess record of the Danube Valley appears to confirm this observation within given chronologic uncertainty (13), there is, however, no apparent explanation available as to the cause of this moist interval during GI-7.
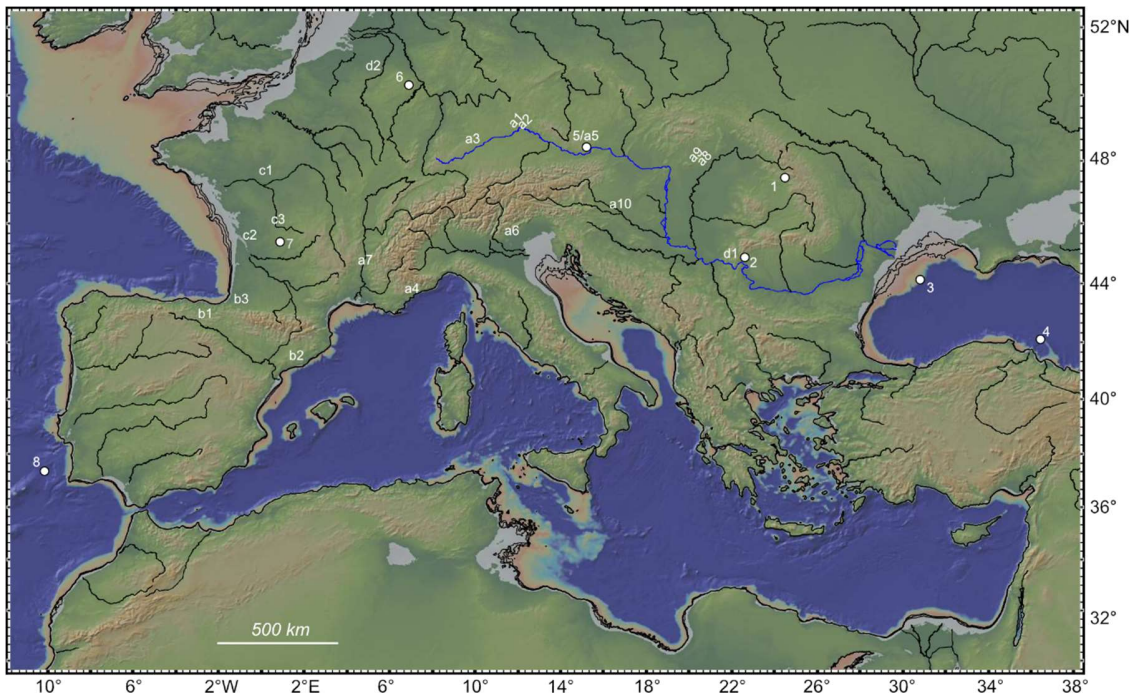
Fig. S1. Map of the southern and central Europe with rivers (blue: the Danube), coastlines for sea level 40 m and 60 m lower than at present, and sites discussed in the main text. Geologic records (dots): (1) Tăuşoare Cave; (2) Ascunsă Cave; (3) core MD04-2790; (4) core M72/5-25-GC1; (5) Willendorf-II paleosol/loess profile; (6) Eifel Maar Lakes; (7) Villars Cave; (8) core MD95-2042. Archeologic sites: (a1) Sesselfelsgrotte; (a2) Keilberg-Kirche; (a3) Geissenklösterle; (a4) Riparo Mochi; (a5) Willendorf-II; (a6) Grotta di Fumane; (a7) Grotte Mandrin; (a8) Pes-kő Cave; (a9) Szeleta Cave; (a10) Vindija Cave; (b1) Labeko Koba; (b2) Abric Romani; (b3) Isturitz; (c1) Grotte du Renne; (c2) Les Cottés; (c3) Saint Césaire; (d1) Oase Cave; (d2) Goyet Cave. The map was generated with the GeoMapApp software, http://www.geomapapp.org (14).

A Stalagmite 1152, Tăușoare Cave, age model

B Stalagmite POM1, Ascunsă Cave, age model
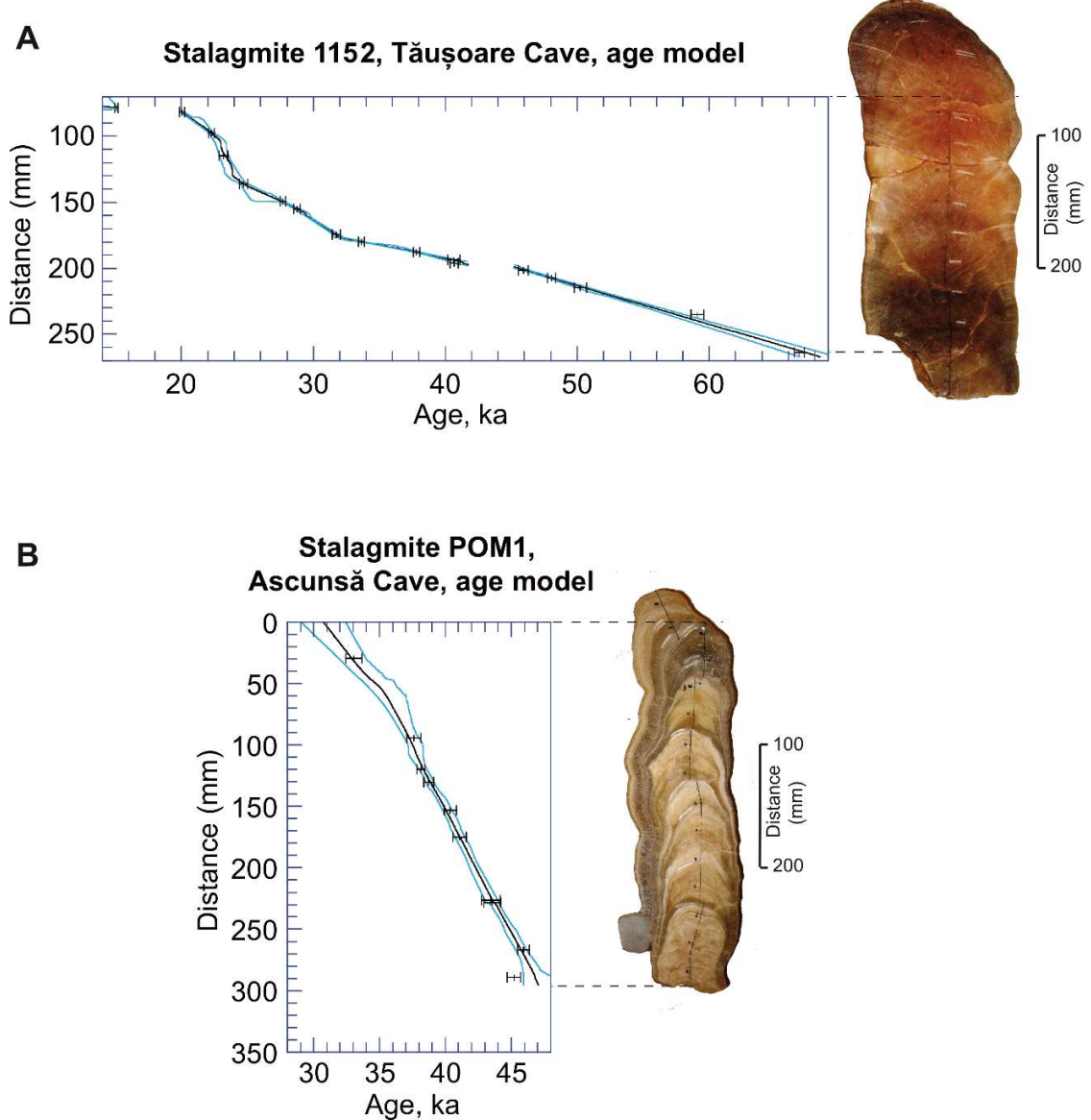
**Fig. S2.** U-Th age models and photographs of a) stalagmite 1152, Tăușoare Cave, and b) stalagmite POM1, Ascunsă Cave.
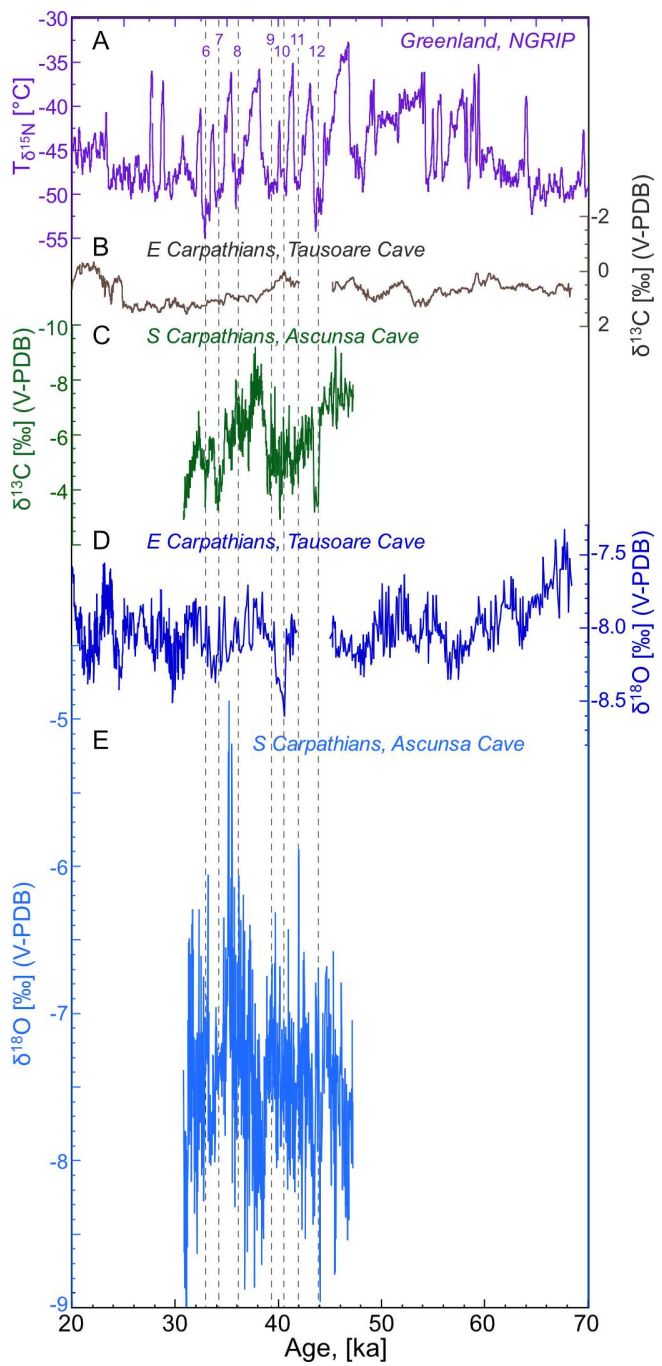
Fig. S3. A: Greenland NGRIP ice core temperatures on the GICC05 time scale with numbered interstadials (8). B: δ¹³C of stalagmite 1152 from Tăușoare Cave. C: δ¹³C of stalagmite POM1 from Ascunsă Cave. D: δ¹⁸O of stalagmite 1152 from Tăușoare Cave. E: δ¹⁸O of stalagmite POM1 from Ascunsă Cave.
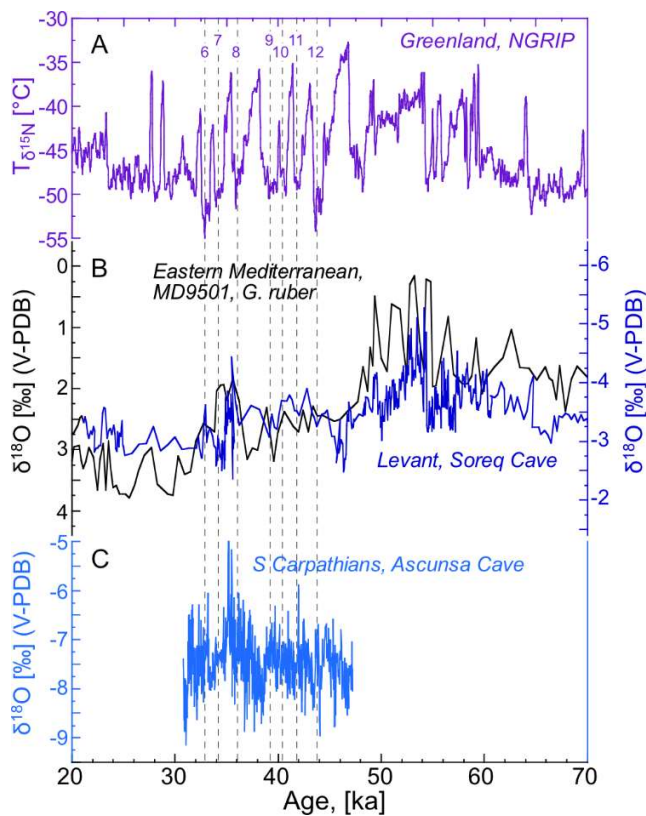
Fig. S4. A: Greenland NGRIP ice core temperatures on the GICC05 time scale with numbered interstadials (8). B: Eastern Mediterranean and Levantine records (10): $\delta^{18}O$ data of planktonic foraminifera (G. ruber) from eastern Mediterranean marine sediment core MD9501, and $\delta^{18}O$ data of a stalagmite from Soreq cave (Israel). C: $\delta^{18}O$ data of stalagmite POM1 from Ascunsă Cave. Note that the scale for the two stalagmites is inverted with respect to each other.

Table S1. U-Th data for stalagmites POM1, Ascunsă Cave, and 1152, Tăuşoare Cave. Corrected values include detrital Th correction.

Sample	Distance (mm)	^{238}U (ng/g)	±	^{232}Th (ng/g)	±	(^{230}Th/^{232}Th) activity ratio	±	(^{230}Th/^{238}U) activity ratio	±	(^{234}U/^{238}U) activity ratio	±	uncorrected age (ka)	±	corrected age (ka)	±	(^{234}U/^{238}U) initial activity ratio	±	Comments
1152 top	0,50	1019,5	6,6	3,442	0,034	6,31	0,15	0,0070	0,0002	1,4296	0,0024	0,53	0,01	0,47	0,04	1,4305	0,0024	
1152 / XIII	16,25	963,1	34,4	3,054	0,467	97,29	1,28	0,1009	0,0038	1,4464	0,0033	7,87	0,30	7,81	0,30	1,4567	0,0034	
1153 / XII	37,38	1304,6	50,9	2,486	0,125	235,37	2,60	0,1468	0,0013	1,5133	0,0035	11,08	0,10	11,04	0,11	1,5298	0,0036	
1152 / XI	38,88	1231,0	40,9	1,438	0,054	404,15	5,16	0,1545	0,0016	1,5394	0,0039	11,48	0,13	11,46	0,13	1,5573	0,0040	
1152 / X	78,50	2632,7	73,8	1,672	0,062	1069,73	15,75	0,2223	0,0019	1,7095	0,0036	15,07	0,14	15,06	0,14	1,7405	0,0037	
1152 / IX	81,50	952,4	28,6	2,950	0,101	306,65	2,91	0,3108	0,0027	1,8252	0,0044	20,10	0,19	20,06	0,20	1,8740	0,0045	
1152 / VIII	97,63	1854,4	70,8	3,301	0,259	578,76	7,41	0,3371	0,0028	1,7996	0,0060	22,31	0,22	22,28	0,22	1,8520	0,0062	
1152 / VII	114,88	1674,3	61,1	1,603	0,552	1061,09	7,72	0,3323	0,0045	1,7126	0,0029	23,21	0,35	23,20	0,35	1,7610	0,0031	
1152 / VI	135,88	942,6	33,0	1,656	0,279	583,06	4,91	0,3352	0,0034	1,6309	0,0050	24,75	0,29	24,72	0,29	1,6769	0,0052	
1152 XXII	149,63	1086,5	53,1	1,051	0,054	1161,09	11,40	0,3674	0,0025	1,6158	0,0034	27,71	0,22	27,69	0,22	1,6661	0,0036	
1152 / V	155,00	1397,5	39,1	1,318	0,040	1151,27	11,89	0,3552	0,0024	1,5133	0,0037	28,77	0,24	28,75	0,24	1,5568	0,0039	
1152 /IV	174,63	931,3	30,0	2,383	0,085	472,40	4,68	0,3955	0,0031	1,5418	0,0034	31,80	0,30	31,75	0,30	1,5931	0,0037	
1152 XVII	179,88	802,2	16,3	1,246	0,047	802,42	22,17	0,4078	0,0022	1,5125	0,0031	33,68	0,22	33,65	0,22	1,5639	0,0033	
1152 XVI	187,88	612,2	13,9	3,442	0,122	243,85	6,17	0,4486	0,0023	1,5034	0,0033	37,91	0,25	37,80	0,25	1,5610	0,0035	
1152 / III	193,63	517,7	21,8	7,404	0,315	101,37	1,00	0,4744	0,0041	1,4903	0,0049	40,92	0,45	40,66	0,47	1,5521	0,0054	
1152 XXI	196,25	506,4	12,8	3,987	0,106	188,71	1,28	0,4862	0,0029	1,5296	0,0031	40,81	0,31	40,67	0,31	1,5953	0,0034	
1152 XV	201,25	566,7	14,1	3,243	0,093	269,37	3,24	0,5044	0,0031	1,4390	0,0033	46,02	0,37	45,91	0,37	1,5006	0,0036	
1152 XIV	207,25	639,8	12,8	2,372	0,052	433,22	3,25	0,5255	0,0023	1,4452	0,0030	48,12	0,29	48,05	0,29	1,5105	0,0033	
1152 / II	215,00	570,5	16,6	3,212	0,100	292,59	2,68	0,5389	0,0039	1,4293	0,0040	50,36	0,48	50,25	0,49	1,4955	0,0044	
1152 / I	234,88	1182,4	38,7	6,035	0,229	360,50	2,83	0,6021	0,0035	1,4059	0,0034	59,21	0,49	59,11	0,49	1,4803	0,0038	
1152/ base	264,00	622,8	3,5	5,433	0,033	225,32	0,50	0,6432	0,0023	1,3694	0,0027	66,98	0,37	66,81	0,38	1,4472	0,0031	
POM 1 / top		32,5	0,2	0,576	0,005	22,93	0,51	0,1331	0,0031	1,2610	0,0040	12,14	0,30	11,74	0,36	1,2710	0,0041	outside measured profile
POM 1 / III	29,67	38,1	0,2	1,923	0,017	20,95	0,18	0,3460	0,0028	1,2746	0,0032	34,18	0,34	33,07	0,61	1,3055	0,0040	
POM1/X	94,33	45,2	0,3	0,164	0,005	292,85	3,83	0,3472	0,0040	1,1799	0,0044	37,69	0,54	37,61	0,54	1,2003	0,0048	
POM 1 / V	119,67	84,8	0,4	0,620	0,006	140,69	1,06	0,3366	0,0021	1,1306	0,0027	38,32	0,31	38,14	0,32	1,1457	0,0030	
POM1/VIII	130,33	70,1	0,4	0,183	0,006	422,27	5,43	0,3602	0,0027	1,1942	0,0036	38,79	0,38	38,73	0,38	1,2168	0,0039	
POM1/VII	153,33	37,3	0,2	0,313	0,003	160,76	1,64	0,4406	0,0038	1,3985	0,0047	40,53	0,45	40,37	0,46	1,4477	0,0051	
POM1/XI	175,33	27,7	0,1	0,079	0,002	473,33	5,60	0,4390	0,0042	1,3776	0,0048	41,13	0,50	41,07	0,50	1,4244	0,0052	
POM 1 / II	226,67	27,7	0,2	0,386	0,004	104,84	1,52	0,4777	0,0063	1,4225	0,0040	43,73	0,71	43,46	0,72	1,4794	0,0045	
POM 1 / I	228,33	20,9	0,1	0,396	0,004	80,09	1,01	0,4955	0,0056	1,4684	0,0050	43,91	0,63	43,56	0,64	1,5324	0,0056	
POM 1 XXII	267,00	24,3	0,1	0,239	0,003	149,77	1,29	0,4825	0,0035	1,3771	0,0031	46,11	0,43	45,92	0,43	1,4304	0,0034	
POM 1 XXIII	289,00	26,4	0,1	0,236	0,006	162,37	1,71	0,4752	0,0042	1,3742	0,0036	45,38	0,51	45,20	0,51	1,4262	0,0040	
POM 1 /base		33,2	0,2	29,626	0,162	2,47	0,02	0,7209	0,0054	1,3700	0,0036	78,29	0,88	59,06	7,83	1,5708	0,0819	discarded from age model

Table S2. Published ^{14}C ages of archaeologic sequences included in Figure 3 and discussed in the text.

site	map signature (Fig. S1)	stratigraphic position / layer	chronologic position in sequence	sample	material	conventional 14C age, ka	ka, cal BP (*p* = 68%, INTCAL13), original calibration (c) / Bayesian model (m); recalibrated (r)	preceding layer, min age ka, cal BP (*p* = 68%)	lower layer boundary ka, cal BP (*p* = 68%)	upper layer boundary ka, cal BP (*p* = 68%)	succeding layer, max age ka, cal BP (*p* = 68%)	Reference	original authors' artifact identification
Grotte du Rennes at Arcy-sur-Cure	c1	VII	oldest	EVA-95	bone	34.81 ± 0.21	39.5 - **40.3** (m)					15	Protoaurignacian
		VIII	model transition VIII/VII	Bayesian model age			40.7 - 41.4 (m)						Chatelperronian, low artifact density
			model transition IX/VIII	Bayesian model age			41.2 - 41.6 (m)						
		IX	youngest	EVA-29	bone	35.50 ± 0.22	**41.0** - 42.1 (m)						Chatelperronian
		summary VIII						**41.0**	41.6	40.7	**40.3**		
Saint Cesaire	c2	ejo sup	n.a.				n.a.					16	Aurignacian 0
		ejop sup / ejo inf	model transition	Bayesian model age			**39.7** - 41.1 (m)						sterile (ejo inf)
		ejop sup	youngest	OxA-21699	bone	36.00 ± 0.70	40.3 - 41.3 (m)						Chatelperronian
		summary ejo inf						41.3	**41.1**	**39.7**	n.a.		
Les Cottes	c3	4	oldest	S-EVA 9713	bone	35.15 ± 0.28	39.3 - **40.0**					17	Protoaurignacian
		5/4	upper boundary	Bayesian model age			39.5 - 40.3 (m)						sterile (layer 5)
		6/5	lower boundary	Bayesian model age			40.8 - 41.6 (m)						
		6	youngest	S-EVA 13666	bone	36.23 ± 0.21	**41.3** - 41.7 (m)						Chatelperronian
		summary 5						41.3	41.6	39.5	**40.0**		
Europe	-			Bayesian age model			**40.0 - 40.8**		40.8	40.0		16	Neanderthal disappearance
Labeko Koba	b1	VII	oldest	OxA-21766	bone	36.85 ± 0.80	41.0 - **41.6** (m)					18	Protoaurignacian
		VIII / VII	upper boundary	Bayesian model age			41.4 - 42.0 (m)						
		VIII	n.a.										sterile
		IX-upper	youngest	OxA-21972	bone	36.55 ± 0.75	41.6 - 42.1 (m)						
		IX-upper	oldest	OxA-23199	bone	38.40 ± 0.90	41.7 - 42.2 (m)						
		IX-lower / IX-upper	lower boundary				41.9 - 42.4 (m)						
		IX-lower	youngest	OxA-22560	bone	37.40 ± 0.80	**42.2** - 42.6 (m)						Chatelperronian
		summary IX-upper						**42.2**	42.2	41.6	**41.6**		

Table S2 continued. Published ^{14}C ages of archaeologic sequences included in Figure 3 and discussed in the text.

site	map signature (Fig. S1)	stratigraphic position / layer	chronologic position in sequence	sample	material	conventional 14C age, ka	ka, cal BP (*p* = 68%, INTCAL13), original calibration (c) / Bayesian model (m); recalibrated (r)	preceding layer, min age ka, cal BP (*p* = 68%)	lower layer boundary ka, cal BP (*p* = 68%)	upper layer boundary ka, cal BP (*p* = 68%)	succeding layer, max age ka, cal BP (*p* = 68%)	Reference	original authors' artifact identification
Abric Romani	b2	A	oldest	OxA-X-2095-46	shell	36.09 ± 0.23	41.3 - **41.7** (m)					19	Aurignacian 0
		AR3/AR6	av. U-series	Bayesian model age			41.6 - 42.6 (U-Th age)						sterile
		B	youngest	OxA-12025	shell	39.06 ± 0.35	**42.8** - 43.5 (m)						Mousterian
		summary AR3/AR6						**42.8**	42.8	41.7	**41.7**		
Sesselfelsgrotte	a1	E3		GrN-7153	charcoal	37.1 ± 1.1	40.7 - **42.3** (r)					20	MMO
		G1		GrN-6848	charcoal	41.84 ± 1.10	44.2 - 46.2 (r)						Mousterian
		G1		GrN-20302	bone	39.95 ± 0.92	42.9 - 44.4 (r)						
		G1		GrN-20303	bone	41.37 ± 1.06	43.6 - 45.7 (r)						
		G1		GrN-21528	combined bone from GrN-20302 & 20303	41.39 ± 0.58	**44.3** - 45.4 (r)						
		summary F						44.3	n.a	n.a	42.3		
Keilberg	a2	layer 2, base		KN-4690	charcoal	37.50 ± 1.45	40.5 - 42.9 (r)					21	Aurignacian
				KN-4691	charcoal	37.50 ± 1.25	40.7 - 42.8 (r)						
				KN-4692	charcoal	38.6 ± 1.20	41.7 - 43.6 (r)						
Geissenklösterle	a3	16	oldest	OxA-21722	bone		41.8 - 42.7 (m)					22	Early Aurignacian
		17/16	upper boundary				42.4 - 43.7 (m)						
		17		OxA-21658	bone		**42.4** - 43.3 (m)						sterile
		17		OxA-21657	bone		42.4 - **43.4** (m)						
		18/17	lower boundary				42.5 - 44.8 (m)						
		18	youngest	OxA-21720	bone		42.5 - 44.5 (m)						Mousterian
		summary 17						42.5	**43.4**	**42.4**	42.7		
Riparo Mochi	a4	G	oldest	Rome-2	charcoal	37.4 ± 1.3	41.4 - 42.3 (m)					23	Protoaurignacian
		transition H/G	range	Bayesian model age			**41.6** - 42.8 (m)						sterile
		transition I/H	range	Bayesian model age			41.8 - **44.0** (m)						Mousterian
		summary H						n.a.	**44.0**	41.6	42.2		
Willendorf	5/a5	C8.2		average of 9 OxA & GrA dates	charcoal		41.7 - **42-9** (c)					24	Early Aurignacian
		C9		n.a.			n.a.						
		D1		average of 9 OxA & GrA dates	charcoal		**43.9** - 46.6 (c)						IUP
		summary C9							**43.9**	42.9			

References

1. Onac BP, Drăguşin V, Papiu F, Theodorescu C-T (2019) Rodna Mountains: Izvorul Tăusoarelor Cave (Pestera de la Izvorul Tăusoarelor). *Cave and Karst Systems of Romania*, eds Ponta GML, Onac BP (Springer International, Cham), pp 47–56.
2. Onac BP, White WB, Viehmann I (2001) Leonite [$K_2Mg(SO_4)_2 \cdot 4H_2O$], konyaite [$Na_2Mg(SO_4)_2 \cdot 5H_2O$] and syngenite [$K_2Ca(SO_4)_2 \cdot H_2O$] fromTausoare Cave, Rodnei Mts, Romania. *Min Mag* 65(1):103-109.
3. Drăguşin V, Vlaicu M, Isverceanu E (2019) Mehedinti Mountains: The Cave from Mohilii Creek (Ascunsă Cave). *Cave and Karst Systems of Romania*, eds Ponta GML, Onac BP (Springer International, Cham), pp 171–173.
4. Hoffmann D, et al. (2007) Procedures for accurate U and Th isotope measurements by high precision MC-ICPMS. Int J Mass Spec 264(2-3): 97-109.
5. Scholz D, Hoffmann DL (2011) StalAge – An algorithm designed for construction of speleothem age models. Quat Geochronol 6(3–4):369–382.
6. Dragusin V, et al. (2017) Transfer of environmental signals from the surface to the underground at Ascunsă Cave, Romania. Hydrol Earth Syst Sci 21(10):5357–5373.
7. Drăguşin V, et al. (2014) Constraining Holocene hydrological changes in the Carpathian–Balkan region using speleothem $\delta^{18}O$ and pollen-based temperature reconstructions. Clim Past 10(4):1363–1380.
8. Rasmussen SO, et al. (2014) A stratigraphic framework for abrupt climatic changes during the Last Glacial period based on three synchronized Greenland ice-core records: refining and extending the INTIMATE event stratigraphy. Quat Sci Rev 106:14–28.
9. Kindler P, et al. (2014) Temperature reconstruction from 10 to 120 kyr b2k from the NGRIP ice core. Clim Past 10(2):887–902.
10. Almogi-Labin A, et al. (2009) Climatic variability during the last ~90ka of the southern and northern Levantine Basin as evident from marine records and speleothems. Quat Sci Rev 28:2882-2896.
11. Hofer D, et al. (2012) Simulated winter circulation types in the North Atlantic and European region for preindustrial and glacial conditions: Glacial Circulation Types. Geophys Res Lett 39(15): DOI 10.1029/2012GL052296.
12. Rowe PJ et al. (2012) Speleothem isotopic evidence of winter rainfall variability in northeast Turkey between 77 and 6 ka. Quat Sci Rev 45:60-72.
13. Obreht I, et al. (2017) Shift of large-scale atmospheric systems over Europe during late MIS 3 and implications for Modern Human dispersal. Sci Rep 7:5848.
14. Ryan, W.B.F, et al (2009) Global Multi-Resolution Topography synthesis, Geochem. Geophys. Geosyst., 10, Q03014, doi:10.1029/2008GC002332.
15. Hublin J-J, et al. (2012) Radiocarbon dates from the Grotte du Renne and Saint-Césaire support a Neanderthal origin for the Châtelperronian. *Proc Natl Acad Sci U S A* 109(46):18743–18748.
16. Higham T, et al. (2014) The timing and spatiotemporal patterning of Neanderthal disappearance. *Nature* 512(7514):306–309.
17. Talamo S, et al. (2012) A radiocarbon chronology for the complete Middle to Upper Palaeolithic transitional sequence of Les Cottés (France). *J Archaeol Sci* 39(1):175–183.
18. Wood RE, et al. (2014) The chronology of the earliest Upper Palaeolithic in northern Iberia: New insights from L'Arbreda, Labeko Koba and La Vina. *J Hum Evol* 69:91–109.
19. Camps M, Higham T (2012) Chronology of the Middle to Upper Palaeolithic transition at Abric Romani, Catalunya. *J Hum Evol* 62(1):89–103.
20. Böhner U (2008) Sesselfelsgrotte IV - Die Schicht E3 der Sesselfelsgrotte und die Funde am Abri Schulerloch (Franz Steiner Verlag Stuttgart, Germany).
21. Uthmeyer T (1996) Ein bemerkenswert frühes Inventar des Aurignacien von der Freilandfundstelle "Keilberg-Kirche" bei Regensburg. *Archaeologisches Korrespondenzblatt* 26:233–248.
22. Higham T, et al. (2012) Testing models for the beginnings of the Aurignacian and the advent of figurative art and music: The radiocarbon chronology of Geißenklösterle. *J Hum Evol* 62(6):664–676.
23. Douka K, et al. (2012) A new chronostratigraphic framework for the Upper Palaeolithic of Riparo Mochi (Italy). *J Hum Evol* 62(2):286–299.
24. Nigst PR, et al. (2014) Early modern human settlement of Europe north of the Alps occurred 43,500 years ago in a cold steppe-type environment. *Proc Natl Acad Sci* 111(40):14394–14399.